J. Chem. Sci. Vol. 123, No. 6, November 2011, pp. 807–818.

Two new 1D chains of Ni_2Na_2 heterometallic double half-cubane building units: Synthesis, structures and variable temperature magnetic study

KARTIK CHANDRA MONDAL[a], BAPPADITYA GOLE[a], YOU SONG[b,*], STUART R BATTEN[c], DAVID R TURNER[c] and PARTHA SARATHI MUKHERJEE[a,*]

[a]Department of Inorganic and Physical Chemistry, Indian Institute of Science, Bangalore 560012, India
[b]State Key Laboratory of Coordination Chemistry, Nanjing University, Nanjing 210093, China
[c]School of Chemistry, Monash University, Australia
e-mail: psm@ipc.iisc.ernet.in; yousong@nju.edu.cn

Abstract. An equimolar mixture of $Ni(NO_3)_2{\cdot}6H_2O$ and pyridine-2-aldehyde with two equivalents of NaN_3 in methanol in the presence of NaOMe resulted in the formation of light green precipitate which upon crystallization from dimethylformamide (DMF) yielded light green single crystals $[\{Ni_2Na_2(pic)_4(N_3)_2(H_2O)_2(MeOH)\}\cdot MeOH{\cdot}3H_2O]_n$ (**1**) and $[\{Ni_2Na_2(pic)_4(N_3)_2(H_2O)_4\}{\cdot}2DMF{\cdot}H_2O]_n$ (**2**) (pic = pyridine-2-carboxylate) at room temperature and high temperature (100°C), respectively. Variable temperature magnetic studies revealed the existence of overall ferromagnetic behaviour with $J \approx +10$ cm^{-1} and $D \approx -2$ to -7 cm^{-1} for **1** and **2**, respectively. Negative D values as well as variation of D upon slight distortion of structure by varying reaction temperature were observed. The X-band Electron Paramagnetic Resonance (EPR) spectra of both **2** and **3** were recorded below 50 K. The structural distortion was also implicated from the EPR spectra. Density Functional Theory (DFT) calculations on both complexes were performed in two different ways to corroborate the magnetic results. Considering only Ni_2^{II} dimeric unit, results were $J = +20.65$ cm^{-1} and $D = -3.16$ cm^{-1} for **1**, and $J = +24.56$ cm^{-1} and $D = -4.67$ cm^{-1} for **2**. However, considering $Ni_2^{II}Na_2^{I}$ cubane as magnetic core the results were $J = +16.35$ cm^{-1} (**1**), $+19.54$ cm^{-1} (**2**); $D = -3.05$ cm^{-1} (**1**), -4.25 cm^{-1} (**2**).

Keywords. Coordination polymers; cluster; Ni_2^{II}, 1D chain; magnetism; DFT.

1. Introduction

After the discovery of exciting single molecular magnetic (SMM) behaviour in Mn_{12}-acetate cluster, metal clusters of different paramagnetic metal ions have been receiving tremendous attention because of their magnetostructural relationship.[1–8] Physical properties (magnetic, optical, etc.) of these materials depend mainly on their structures. Frequently, polymeric magnetic networks also contain repetition of paramagnetic cluster units.[9] Hence, their bulk magnetic nature becomes collective behaviour of cooperative magnetic clustering units. There are several magnetic parameters [spin (S), dipolar, isotropic, anisotropic exchange parameter, zero field splitting (D), etc.] which operate on each other and thus their properties depend on the positions of the paramagnetic spin ions with respect to each other.[10] For a SMM, two most important parameters are of essential criteria: negative D and high S. Usually in paramagnetic clusters, metal ions are linked to each other by diamagnetic bridging ligands and[9,11] the magnetic exchange propagates through those bridging pathways. The coordination geometry and environment of a paramagnetic ion is also very important when magnetic behaviour is concerned as it has direct influence on anisotropy (D) parameter.[12]

Since paramagnetic metal ions (Ln^{III}, Mn^{III}, Co^{II}, Ni^{II}, Cr^{II}, etc.) contain considerable amount of single-ion magnetic anisotropy, the effect of which on their magnetic behaviour of a cluster is obvious.[13,14] Healthy contribution of S and D can bring up exciting magnetic behaviour in a magnetic system. Thus synthesis of new clusters, their magneto-structural correlation and extraction of their magnetic parameters are very important in order to enrich the literature and make the understanding better. Since Ni^{II} ion contains considerable single-ion magnetic anisotropy, Ni_2^{II} clusters are of considerable attention. Some Ni_2^{II} discrete complexes such as $[(Ni_2^{II}(en)Cl_2]Cl_2$[15–18], $\{Ni_2^{II}(N_3)_2\}$[19] and $\{Ni_2^{II}(OR)_2\}$[20] were characterized and magnetic properties were investigated. In case of $[(Ni_2^{II}(en)Cl_2]Cl_2$[18] authors elucidated the microscopic origin of ZFS in dinuclear (Ni_2^{II}) exchange coupled systems with large anisotropy and first time experimentally and theoretically extracted D_{AB}

*For correspondence

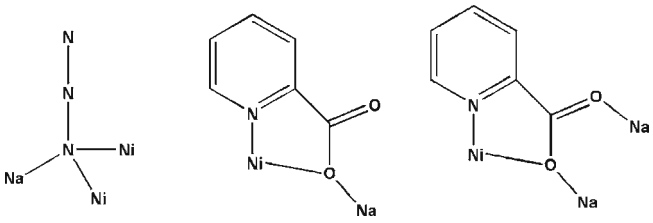

Scheme 1. The 1,1,1 bridging mode of azide (left) and bridging modes of picolinate observed in **1** (center) and **2** (right).

(asymmetric exchange parameter) of a Ni_2^{II} cluster. This result on Ni_2^{II} dimer helped to have better understanding on more complicated systems such as Ni_4^{II} [21–28], Ni_6^{II} [29,30], Ni_{12}^{II} [31], $Na_6^{I}Ni_{16}^{II}$ [32] which are constructed by assembling Ni_2^{II} units. The density functional theory (DFT) calculation was used on Ni_2^{II} [27,28] and Ni_4^{II} [26] complexes to get better ideas on magnetic and optical properties. [23,33]

Being inspired by the above mentioned facts, we used pyridine-2-aldehyde as a blocking agent and sodium azide as a magnetic coupler[34–37] in combination with Cu^{II} or Ni^{II} cations in methanol medium. The former yielded a defect cubane $[Cu_4\{PyCH(O)(OMe)\}_4(N_3)_4]$[38] {PyCH(O)(OMe) = pyridine-2-hemiacetal} cluster while the latter reaction produced 1D heterometallic chains $[\{Ni_2Na_2(pic)_4(N_3)_2(H_2O)_2(MeOH)\}\cdot MeOH\cdot 3H_2O]_n$ (**1**) and $[\{Ni_2Na_2(pic)_4(N_3)_2(H_2O)_4\}\cdot 2DMF\cdot H_2O]_n$ (**2**) (pic = pyridine-2-carboxylate) depending upon the reaction condition. Similar reaction using $Cu(NO_3)_2\cdot 3H_2O$ and NaOMe yielded a known heterometallic polymer $[NaCu(pic)(N_3)_2]_n$.[39] In case of **1** and **2**, pyridine-2-aldehyde was oxidized to picolinic acid. Picolinate anion bridged between Ni^{II} and Na^{I} (scheme 1) in **1** and **2**. Here we also report the magnetic properties, X-band EPR and DFT calculations to corroborate the magnetic results of the 1D heterometallic chains **1** and **2**.

2. Experimental

2.1 *Materials and methods*

Pyridine-2-aldehyde, $Ni(NO_3)_2\cdot 6H_2O$, NaN_3 and NaOMe are commercially available and were used as received without any further purification. All solvents were commercially available and used as received.

2.2 *Physical measurements*

Elemental analyses (C, H, N) were performed using a Perkin-Elmer 240C analyzer. IR spectra were recorded in the range 4000–400 cm^{-1} in FT-IR spectrometer using KBr pellets. The variable temperature magnetic studies were carried out on crystalline samples using a Quantum Design SQUID magnetometer. The experimental susceptibilities were corrected for diamagnetism (Pascal's tables).

Caution! Azide complexes are potentially explosive in the presence of organic ligands. Only a small amount of the material should be prepared and handled with care.

2.3 *Synthesis of* $[\{Ni_2Na_2(pic)_4(N_3)_2(H_2O)_2(MeOH)\}\cdot MeOH\cdot 3H_2O]_n$ (**1**)

Pyridine-2-aldehyde (107 mg, 1 mmol) and $Ni(NO_3)_2\cdot 6H_2O$ (290.8 mg, 1 mmol) were taken in 5 mL of methanol and solid NaOMe (54 mg, 1 mmol) was added to the resulting solution to form a green solution. The resultant solution was layered with aqueous solution (2 mL) of NaN_3 (130 mg, 2 mmol). Microcrystalline green product was appeared at the junction. Light green block shaped crystals of **1** were formed in about three weeks from the DMF solution of the microcrystalline solid product. Isolated yield: 30%. Anal calcd for $C_{26}H_{34}N_{10}O_{15}Na_2Ni_2$: C, 35.08; H, 3.85; N, 15.73; Found: C, 35.32; H, 3.59; N, 16.05. IR bands (cm^{-1}): 3457, 2065, 1671, 1638, 1598, 1568, 1385, 1293, 1023, 769, 703.

2.4 *Synthesis* $[\{Ni_2Na_2(pic)_4(N_3)_2(H_2O)_4\}\cdot 2DMF\cdot H_2O]_n$ (**2**)

Pyridine-2-aldehyde (107 mg, 1 mmol) and $Ni(NO_3)_2\cdot 6H_2O$ (290.8 mg, 1 mmol) were taken in 5 mL of methanol and solid NaOMe (54 mg, 1 mmol) was added to the resulting solution to form a green solution. An aqueous solution of NaN_3 (130 mg, 2 mmol) was added slowly with continuous stirring for 15 min. Microcrystalline green product was formed in half an hour. The solid product was dissolved in a mixture of DMF (10 mL), MeOH (7 mL) and water (2 mL) and heated at 100°C for 12 h in a Teflon lined hydrothermal bomb. Slow evaporation of the resulting solution led to the isolation of nice block shaped green crystals of **2** within a week. Isolated yield: 65% Anal calcd: C, 37.03; H, 4.11; N, 17.28; Found: C, 36.68; H, 3.78; N, 17.22. IR (cm^{-1}): 3457, 2064, 1671, 1637, 1597, 1568, 1384, 1293, 1023, 769, 703.

2.5 *Crystal structure determination*

Single crystals were mounted on a Bruker Apex-II CCD diffractometer equipped with graphite monochromated

Mo-Kα radiation ($\lambda = 0.71073$ Å). The SMART program was used for data acquisition, and the SAINT program was used for data extraction.[40] The structures were solved by direct methods using the SHELX-97[41] incorporated in X-Seed.[42,43] Empirical absorption corrections were applied with SADABS.[44] All non-hydrogen atoms were refined anisotropically and were located on geometrically calculated positions. Single crystal data of **1** and **2** were collected at 150 K and 123 K respectively. A summary of crystal data and structure refinements are listed in table 1. Selected bond parameters for all complexes are assembled in table 2.

2.6 *Computational methodology*

The exchange coupling constants in the reported complexes have been calculated using a phenomenological Heisenberg Hamiltonian $H = -\Sigma J_i S_j.S_k$ (where i labels the different kinds of coupling constants, while j and k refer to the different paramagnetic centres)[45,46] to describe the exchange coupling between each pair of transition-metal ions present in the polynuclear complex. To calculate the exchange coupling constants for the polynuclear complexes with n different exchange constants, the energy of $n + 1$ spin configurations was calculated. In the case of the studied model dinuclear complexes, the exchange coupling value J was obtained by taking into account the energy of two different spin distributions: high spin quintet (Q) with $S = 2$ and low spin singlet with $S = 0$. The following equation has been employed to calculate the exchange coupling constant,[47]

$$J = 2\Delta E/S\,(S+1),\ \Delta E = E_{S(BS)} - E_Q,$$

where ΔE is the energy difference between broken symmetry singlet state ($E_{S(BS)}$) and quintet state (E_Q). The hybrid B3LYP functional[48] has been used in all calculations as implemented in *Gaussian 03* package,[49] mixing the exact Hartree–Fock type exchange with Becke's expression for the exchange functional[50] and that proposed by Lee–Yang–Parr for the correlation contribution.[51] The use of the non-projected energy of the broken-symmetry solution as the energy of the low spin state within the DFT framework provides more or less satisfactory results avoiding the cancellation of the non-dynamic correlation effects.[52] The broken symmetry approach along with electron correlations at the B3LYP level has been widely used to investigate magnetic properties in a large number of magnetic systems. We have considered LANL2DZ basis set for Ni and 6–31G for rest of the atoms.

Table 1. Selected crystal data and refinement details for **1**–**2**.

Compounds	**1**	**2**
Empirical formula	$C_{26}H_{34}N_{10}Na_2Ni_2O_{15}$	$C_{30}H_{40}N_{12}Na_2Ni_2O_{15}$
Formula weight	889.97	972.14
Temperature	150(1) K	123(1) K
Wavelength	0.71073 Å	0.71073 Å
Crystal system	Triclinic	Triclinic
Space group	$P_{\bar{1}}$	$P_{\bar{1}}$
a/Å	11.054(4)	11.1146(5)
b/Å	12.220(5)	12.4973(6)
c/Å	17.138(7)	16.6305(9)
α/°	91.259(7)	99.620(2)
β/°	106.738(7)	109.439(2)
γ/°	115.248(6)	94.908(2)
Volume/Å^3	1976.7(14)	2122.8(2)
Z	2	2
ρ/mgcm^{-3}	1.959	1.521
μ/mm^{-1}	2.335	0.986
Reflns col.	16701	17341
Ind. Reflns/R_{int}	8989/0.0410	9489/0.0275
Final[a] $R[I>2\sigma]/wR_2$	0.0918/0.1834	0.0363/0.0814
R (all data)/wR_2	0.1465/0.2170	0.0507/0.0875

[a] $R = (\Sigma||F_o| - |F_c||)\,/\,\Sigma|F_o|$; $wR_2 = \left[\Sigma\, w\left(F_o^2 - F_c^2\right)/\Sigma\, wF_o^4\right]^{1/2}$

Table 2. Selected bond distances (Å) and angles (°) for **1** and **2**.

		Complex-**1**			
Ni(1)- O(1)	2.024(4)	Ni(1)-N(2)	2.067(5)	$Ni(1)^{\#1}$-N(3)	2.113(5)
$Ni(1)^{\#1}$-Na(2)	3.468(3)	Ni(2)-O(7)	2.041(4)	Ni(2)-O(5)	2.056(4)
Na(1)-Na(2)	3.367(4)	$N(8)-Ni(2)^{\#1}$	2.084(5)	Ni(1)-O(3)	2.028(4)
Ni(1)-N(1)	2.068(5)	Ni(1)-N(3)	2.161(5)	Ni(1)-Na(2)	3.528(3)
Ni(2)-N(7)	2.044(5)	Ni(2)-N(6)	2.064(5)	Ni(2)-N(8)	2.122(5)
Na(2)-Ni(1)	3.528(3)				
O(1)-Ni(1)-O(3)	176.19(2)		O(3)-Ni(1)-N(2)		80.05(2)
O(3)-Ni(1)-N(1)	97.53(2)		$O(1)-Ni(1)^{\#1}$-N(3)		93.80(2)
$N(2)-Ni(1)^{\#1}$-N(3)	167.45(2)		O(1)-Ni(1)-N(3)		88.48(2)
N(2)-Ni(1)-N(3)	92.23(2)		N(3)-Ni(1)-N(3)		82.81(2)
O(7)-Ni(2)-O(5)	171.66(2)		O(7)-Ni(2)-N(6)		93.60(2)
O(5)-Ni(2)-N(6)	79.53(2)		N(7)-Ni(2)-N(8)		165.90(2)
$N(6)-Ni(2)^{\#1}$-N(8)	97.10(2)		$N(7)-Ni(2)^{\#1}$-N(8)		91.70(2)
N(6)-Ni(2)-N(8)	170.30(2)		O(1)-Ni(1)-N(2)		97.59(2)
O(1)-Ni(1)-N(1)	79.52(2)		N(2)-Ni(1)-N(1)		92.36(2)
$O(3)-Ni(1)^{\#1}$-N(3)	88.84(2)		$N(1)-Ni(1)^{\#1}$-N(3)		94.87(2)
O(3)-Ni(1)-N(3)	94.59(2)		N(1)-Ni(1)-N(3)		167.62(2)
O(7)-Ni(2)-N(7)	80.10(2)		N(7)-Ni(2)-O(5)		95.30(2)
N(7)-Ni(2)-N(6)	92.00(2)		$O(7)-Ni(2)^{\#1}$-N(8)		88.59(2)
$O(5)-Ni(2)^{\#1}$-N(8)	96.90(2)		O(7)-Ni(2)-N(8)		95.85(2)
O(5)-Ni(2)-N(8)	91.22(2)		$N(8)-Ni(2)-N(8)^{\#1}$		81.10(2)
		Complex-**2**			
Ni(1)-O(1)	2.041(2)	Ni(1)-O(3)	2.058(2)	$Ni(1)^{\#1}$-N(5)	2.115(2)
Ni(2)-O(7)	2.022(2)	Ni(2)-N(4)	2.054(2)	$Ni(2)^{\#1}$-N(8)	2.117(2)
Na(1)-O(11)	2.269(2)	Na(1)-O(3)	2.409(2)	Ni(1)-N(2)	2.057(2)
Ni(1)-N(1)	2.059(2)	Ni(1)-N(5)	2.119(2)	Ni(2)-O(5)	2.045(1)
Ni(2)-N(3)	2.060(2)	Ni(2)-N(8)	2.139(2)	Na(1)-O(1)	2.357(2)
O(1)-Ni(1)-N(2)	95.69(7)		N(2)-Ni(1)-O(3)		80.25(7)
N(2)-Ni(1)-N(1)	92.63(7)		$O(1)-Ni(1)^{\#1}$-N(5)		88.73(6)
$O(3)-Ni(1)^{\#1}$-N(5)	93.98(6)		O(1)-Ni(1)-N(5)		93.07(7)
O(3)-Ni(1)-N(5)	91.17(7)		N(5)-Ni(1)-N(5)		81.91(7)
O(7)-Ni(2)-N(4)	79.99(7)		O(7)-Ni(2)-N(3)		98.59(7)
N(4)-Ni(2)-N(3)	96.14(7)		$O(5)-Ni(2)^{\#1}$-N(8)		88.24(6)
$N(3)-Ni(2)^{\#1}$-N(8)	165.88(7)		O(5)-Ni(2)-N(8)		92.50(6)
N(3)-Ni(2)-N(8)	91.09(7)		O(1)-Ni(1)-O(3)		175.26(6)
O(1)-Ni(1)-N(1)	79.80(6)		O(3)-Ni(1)-N(1)		97.88(7)
$N(2)-Ni(1)^{\#1}$-N(5)	94.34(7)		$N(1)-Ni(1)^{\#1}$-N(5)		167.11(7)
N(2)-Ni(1)-N(5)	170.41(7)		N(1)-Ni(1)-N(5)		92.78(7)
O(7)-Ni(2)-O(5)	178.08(6)		O(5)-Ni(2)-N(4)		99.30(7)
O(5)-Ni(2)-N(3)	79.68(6)		$O(7)-Ni(2)^{\#1}$-N(8)		93.58(6)
$N(4)-Ni(2)^{\#1}$-N(8)	92.99(7)		O(7)-Ni(2)-N(8)		88.37(6)
N(4)-Ni(2)-N(8)	167.09(7)		$N(8)-Ni(2)-N(8)^{\#1}$		82.09(7)

Symmetry transformations used to generate equivalent atoms: #1 $-$ x + 2, y, $-$z + 1

3. Results and discussion

3.1 *Synthesis*

The reaction of $Cu(NO_3)_2{\cdot}2.5H_2O$ and pyridine-2-aldehyde in 1:1 ratio in methanol in presence of 4-aminopyridine and sodium azide yielded $[Cu_4\{PyCH(O)(OMe)\}_4(N_3)_4]$.[38] The X-ray diffraction established the formation of a Cu_4 defect cubane structure with four hemiacetylate anions $[PyCH(O)(OMe)]^{-1}$, two end-on azides and two terminal azides. Intermediate hemiacetal during the formation of acetal is known to be unstable and thus isolation of hemiacetal is a great challenge to chemist. Complex $[Cu_4\{PyCH(O)(OMe)\}_4(N_3)_4]$ was the first example of the coordination metal cluster of $[PyCH(O)(OMe)]^{-1}$ hemiacetalate.

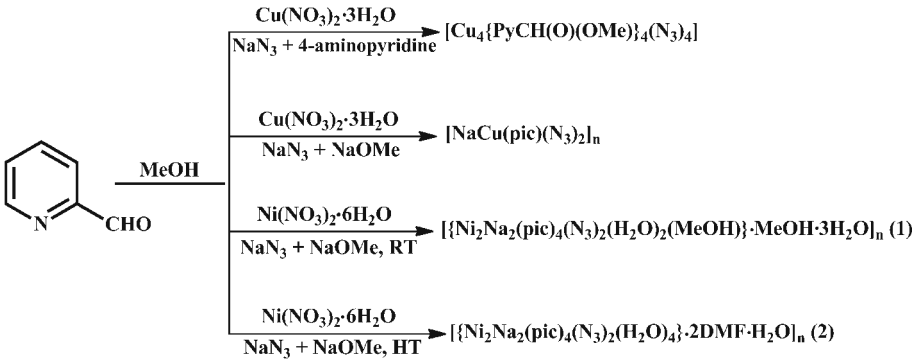

Scheme 2. Synthetic strategy of all the four different complexes.

Inspired by mixed azide and hemiacetylate bridged defect cubane structure of $[Cu_4\{PyCH(O)(OMe)\}_4(N_3)_4]$, a similar kind of reaction was performed using $Ni(NO_3)_2{\cdot}6H_2O$ instead of $Cu(NO_3)_2{\cdot}3H_2O$. However, we were unsuccessful in getting single crystals for further study. Then a slight change in the molar ratio and replacement of 4-aminopyridine by NaOMe (1 mmol) were adopted. X-ray crystal structure of **1** revealed the formation of an 1D chain of defect cubane $Na^{I}_2Ni^{II}_2$ cluster with two Ni^{II} ions in body positions and two Na^{I} ions in the wings. Crystal structure revealed that pyridine-2-aldehyde was oxidized to corresponding pyridine-2-carboxylic acid (picolinic acid). The absorption peaks at 2065, 1671, 1638 and 1385 cm^{-1} in the IR spectrum of the complex **1** are presumably due to the bridging azide and the picolinate, respectively.

Complex **2** was prepared in a slightly different way. The green microcrystalline product obtained after mixing the reactants was dissolved in a mixture of DMF (10 mL), MeOH (7 mL) and water (2 mL) and heated at 100°C for 12 h in a Teflon lined steel bomb. Slow evaporation of the green filtrate in air led to the isolation of green single crystals of **2** in high yield. X-ray crystal structure of **2** revealed an almost similar 1D chain structure of defect cubane type Na_2Ni_2 as repeating unit. The absorption peaks at 2064, 1671 and 1637 cm^{-1} in the IR spectrum of the complex **2** are presumably due to the bridging azide and picolinate carboxylate moieties, respectively. Synthetic strategy of all the complexes is summarized in scheme 2.

Binding of pyridine-2-carboxylaldehyde to the Ni^{II} centre and hydration at the aldehyde-carbon followed by aerial oxidation to acid is a probable mechanism of formation of picolinate. Attempts to obtain **1** and **2** directly using picolinate instead of pyridine-2-aldehyde were failed. However, an analogous reaction using $Cu(NO_3)_2{\cdot}2.5H_2O$ yielded a known heterometallic polymer $[NaCu(pic)(N_3)_2]_n$.[39]

3.2 *Crystal Structure of **1***

From the single crystal X-ray diffraction data it was clear that pyridine-2-aldehyde was oxidized to the corresponding carboxylic acid (picH). The crystallographic asymmetric unit of complex **1** contains two independent $Ni^{II}Na^{I}$ units with two picolinates, one azide, two μ_2-H_2O and a methanol molecule coordinated to one Na(I) ion (figure 1). The coordination geometry around both the Ni(II) centres is distorted octahedral. Two pyridyl nitrogens and two picolinate-oxygens are coordinated to each Ni(II) ion in chelating fashion and the other two coordination sites were occupied by two azido nitrogens. Hence, each Ni(II) has N_4O_2 coordination environment, with bond lengths Ni(1)-N(1) = 2.068(5) Å, Ni(1)-N(2) = 2.067(5) Å, Ni(1)-N(3) = 2.161(5) Å, Ni(1)-O(1) = 2.024(4) Å and Ni(1)-O(3) = 2.028(4) Å. However, each Na^+ ion has O_5N coordination atmosphere. One Na(I) is coordinated to two bridging water, three carboxylate oxygens and one azido nitrogen. The second Na(I) is coordinated to two bridging water, two carboxylate oxygens, one azido nitrogen and one MeOH

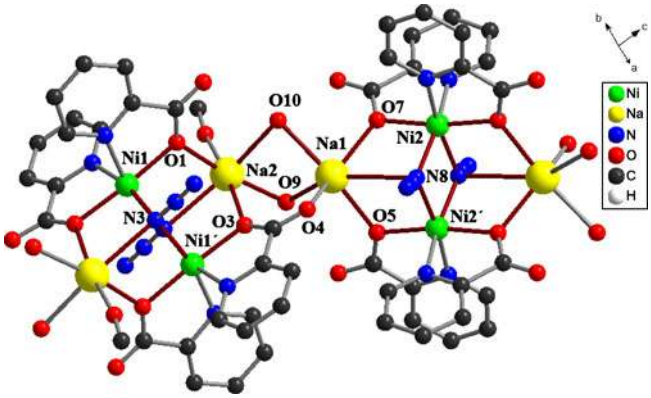

Figure 1. Crystal structure of **1** with atom numbering scheme. Hydrogens are omitted for the sake of clarity.

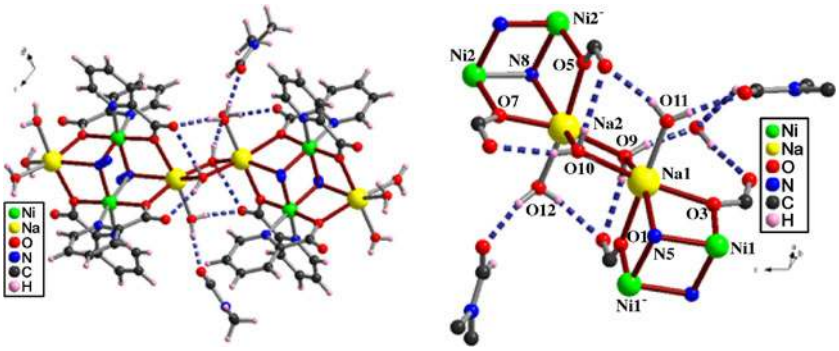

Figure 2. View of the repeating heterometallic $Ni^{II}_2Na^{I}_2$ incomplete dicubane unit in complex **2** (left) and the coordination environment around Na^+ (right). The blue dashed line represents H-bonding.

molecule. The Ni(1)-N(3)(azido)-Ni(1) and Ni(2)-N(8)(azido)-Ni(2) bond angles are 97.19(2)° and 98.9(2)°, respectively, which are in the range for showing ferromagnetic interaction through the end-on azido pathway. Two Na(I) (Na1 and Na2) ions are bridged by two bridging water molecules and a carboxylate group with distance Na(1)-Na(2) = 3.367(4) Å. One MeOH and three water molecules of crystallization were present in the crystal lattice. Several H-bonding between these solvent molecules and two μ-H_2O/picolinates were found in the solid state structure. There is a centre of symmetry between each crystallographic $Ni^{II}Na^{I}$ asymmetric unit. Bridging water and picolinate moieties link the heterometallic defect dicubanes to form a 1D chain structure (figure 1).

3.3 *Crystal Structure of* **2**

The crystal structures of **1** and **2** are closely related except the bridging fashion of the picolinate and the environment around Na(I) centres. The crystallographic asymmetric unit of complex **2** also contains two independent $Ni^{II}Na^{I}$ (figure 2) units. The coordination geometry around both the metal centres in **2** is distorted octahedral. Two picolinates are coordinated to each Ni(II) ion in chelating fashion and the other two sites were satisfied by two azides. Hence, each Ni(II) has N_4O_2 coordination environment. The O_5N coordination environment around each Na^+ is satisfied by coordinated water, two bridging water molecules, two carboxylate oxygens and an azido-nitrogen. There is a centre of symmetry between each crystallographic $Ni^{II}Na^{I}$ asymmetric unit. The X-ray crystallographic packing revealed an one-dimensional (1D) chain structure (figure 3) of the complex **2** formulated as $[\{Ni_2Na_2(pic)_4(N_3)_2(H_2O)_4\}\cdot 2DMF\cdot H_2O]_n$ and this chain consists of two different $Ni^{II}_2Na^{I}_2$ heterometallic defect cubane units which are linked to each other by double μ_2-H_2O bridges. For **1**, two bridging molecules are more bent with respect to two different Ni^{II}_2 dimeric units because of Na(1) site is coordinated by one oxygen-atom (O4) of one picolinate while this coordination site in **2** was satisfied by one water molecule O(12) (figures 2 and 3). Two Ni(II) ions in the basic unit are bridged by two azide ions in end-on fashion and the Na^+ ions are bridged to the Ni^{II}_2 dimeric unit *via* 1,1,1-azido as well as the carboxylate oxygen.

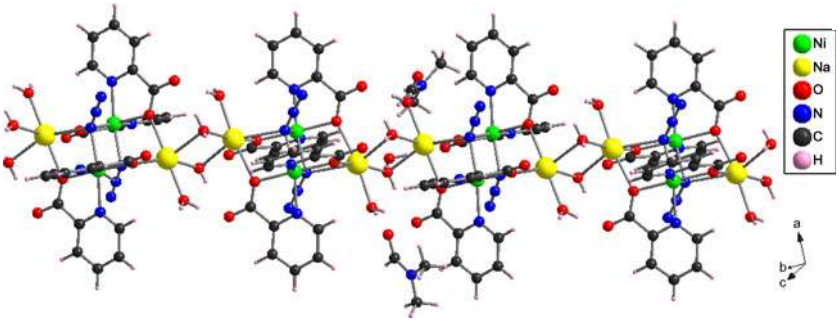

Figure 3. View of the polymeric one-dimensional chain structure of complex **2**.

The lengths of the bonds formed between Ni(II) and two picolinates in **2** are Ni(1)-N(1) = 2.0592(18) Å, Ni(1)-O(1) = 2.0414(15) Å; and Ni(1)-N(2) = 2.0571(19) Å, Ni(1)-O(3) = 2.0582(15) Å, respectively. The 5th and 6th coordination sites are satisfied by two bridging azides binding in end-on fashion with bond lengths of Ni(1)-N(5) = 2.1193(18) Å and Ni(1)-N(5) = 2.1148(17) Å, respectively. The Ni-N(azido)-Ni bond angle is 98.09(7)° which is in the range for showing ferromagnetic interaction through the end-on azido pathway. The coordination view around the Ni(II) centres is shown in figure 2. Na^+ ions in the one-dimensional chain are also found to occupy octahedral coordination geometry. Each Na(I) ion is linked to Ni(II) centre through the bridging carboxylate moiety of two picolinates with the bond angles Na(1)-O(1)-Ni(1) = 103.67(6)° and Na(1)-O(3)-Ni(1) = 100.62(7)°. The 3rd coordination position is occupied by the azide group which acts as a bridge between the Ni(II) and Na(I) ions with bond length Na(1)-N(5) = 2.559(2) Å. Three water molecules occupy the other three coordination positions. The complex was crystallized with water and DMF as solvents of crystallization. Aromatic π–π interaction between the picolinates and hydrogen-bonding interaction through water molecules link the neighbouring chains.

The overall packing view (figure 4) shows the formation of two different pockets one of which is occupied by water molecules while the other one hosted DMF molecules. Interestingly, these pockets are repeating in an alternate ABAB fashion in both the crystallographic *b* and *c* directions. Both complexes are stable in air for few minutes but lose crystallinity afterward probably because of loss of solvents molecule.

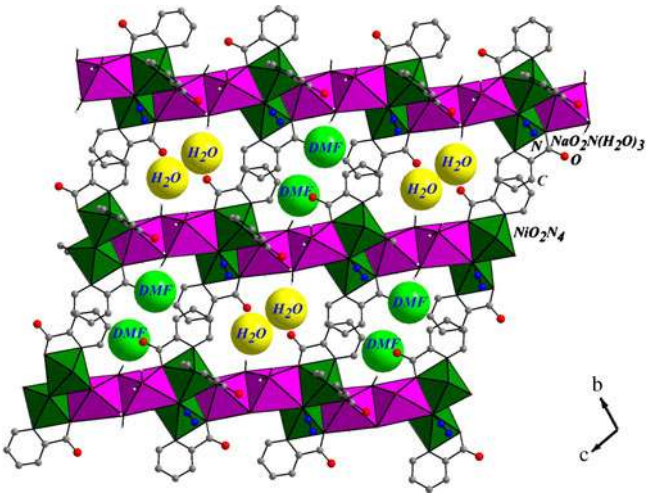

Figure 4. Two-dimensional packing view of the chains in the solid state of complex **2**.

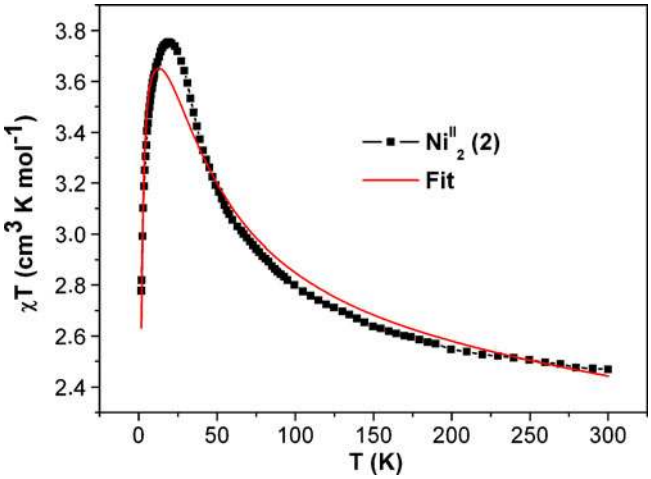

Figure 5. Plot of χT *vs* T of **1** at 1000 Oe applied magnetic field.

3.4 *Magnetic behaviour*

The temperature dependence magnetic susceptibilities were measured on powder samples of $Ni^{II}_2Na^{I}_2$ (**1**) and $Ni^{II}_2Na^{I}_2$ (**2**) in the temperature range of 1.8–300 K under an applied dc magnetic field of 1000 Oe. At room temperature, the experimental χT values of **1** and **2** are 2.46 and 2.57 cm^3 K mol^{-1} respectively, (figures 5 and 6) are slightly more than the expected value of 2.0 cm^3 K mol^{-1} for an uncoupled Ni^{II} ion (with g = 2, S = 1).[13,53]

The values of χT of **1** and **2** increase gradually from 300 K to 100 K and then rapidly with further cooling (figures 5 and 6) and reach maxima at 19 K (3.76 cm^3 K mol^{-1}) and 12 K (3.45 cm^3 K mol^{-1}) before further fall to 2.78 and 3.02 cm^3 K mol^{-1}, respectively. The initial increase indicates ferromagnetic exchange interactions between the Ni^{II} ions, while the

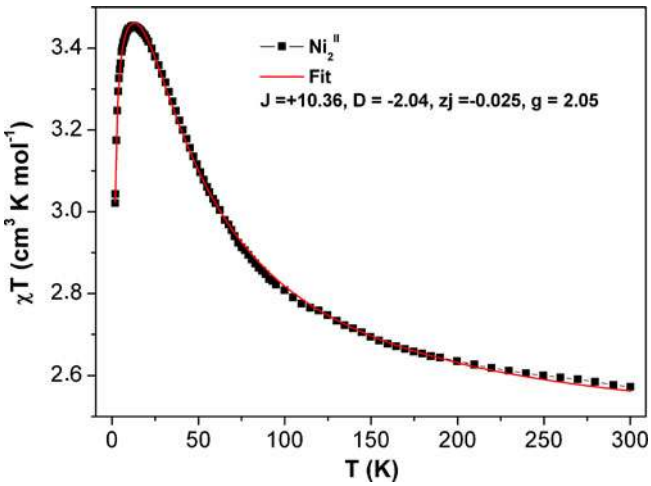

Figure 6. Plot of χT *vs* T of **2** at 1000 Oe applied magnetic field.

decrease at lower temperature region can be ascribed to the ZFS of the ground state or due to intermolecular antiferromagnetic interaction.

The magnetic data were analysed using the Ginsberg's model, considering the isotropic spin-coupling Hamiltonian[15,17]

$$H = -2JS_1 \cdot S_2 - D\left(S_{1z}^2 + S_{2z}^2\right) - g_i \mu_B H \cdot S_i,$$

where i = x, y or z. The term D (single-ion magnetic anisotropy) represents the usual zero-field splitting of the $^3A_2$ ground state of nickel(II).[12,13]

The expression for the susceptibility[15,16] used for fitting the magnetic data is given in supporting information.

The inter-dimer interaction was taken into account by mean field theory.

$$\chi_M^{\text{int}\,er-\text{dim}\,er} = \frac{\chi_A^{\text{dim}\,er}}{1 - \frac{2ZJ'}{g^2 N_A \beta^2}\chi_A^{\text{dim}\,er}} + (\alpha)TIP.$$

The best-fit parameters obtained for **1** using the above expression are $J = +10.28(2)$ cm^{-1}; $D = -7.20(4)$ cm^{-1}; $zJ' = -0.015(4)$ cm^{-1} g = 2.0, $TIP = 3 \times 10^{-6}$ and R = 3×10^{-3} (figure 5). While for **2** the parameters are $J = +10.36(2)$ cm^{-1}; $D = -2.04(3)$ cm^{-1}; $zJ' = -0.025(4)$ cm^{-1} g = 2.05, $TIP = 2 \times 10^{-6}$ and R = 3×10^{-4} (figure 6). Similar D values for Ni(II) systems were reported earlier.[18,20] The presence of moderately strong ferromagnetic interaction in the molecule can be easily attributed due to the Ni(1/2)-N(azido)-Ni(1/2) bond angles of 97.19(19)° and 98.9(2) for **1** and 98.09(7)° and 97.91(7)° for **2**, which are far below the angle 108° above which end-on azido bridged Ni(II) complexes show antiferromagnetic interaction.[53] The magnetic data were also fitted using the model of isolated Ni_2 dimer (no-intermolecular interaction) considering no zero-field-splitting parameter but did not produce satisfactory fit. The fittings to the different models considering J, zJ' and D were performed and best fittings are shown in figures S2 and S3 (for complexes **1** and **2** respectively). Some plots with different J and D were simulated (see Supporting Information, figures S4–S7) in order to compare with that of **1** and **2**. The fitting of magnetic data of **1** in the low temperature region was not fully satisfactory, which could be due to non-inclusion of D_{AB} parameter in Ginsberg's model.[15–18]

The field dependence of magnetization for both **1** and **2** at 2 K increases with increasing dc field and reaches saturation of magnetization [μ_B = 4.04 (**2**) and 4.05 (**3**)] at 7 T (figures 7 and 8). The expected saturated magnetization (M_s) value (with S = 2, g = 2.0) is 4 μ_B if both the Ni^{II} (g = 2) ions are ferromagnetically coupled. Moreover, the M *vs* H/T plots of **1** at low

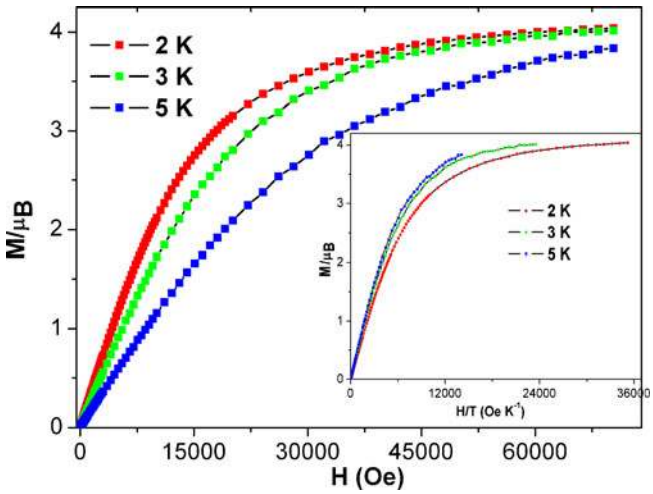

Figure 7. Plots of M *vs* H and H/T (inset) of **1** at indicated temperatures.

temperatures (figure 7, inset) are not superimposed on a single master-curve as expected for anisotropic system, which indicates the presence of magnetic anisotropy and/or low lying excited states.[14] While, the M *vs* H/T plots at low temperatures (figure 8, inset) for **2** are almost superimposed on a single master-curve as expected for a weakly anisotropic system. The best-fit of M *vs* H plots using Brillion function[13] for **1** and **2** at 2 K are provided in Supporting Information (figures S9–S10). Since very small structural changes can significantly change the energy diagram of the magnetic orbitals, EPR measurement and DFT calculations were done in order to get more accurate insight on the magnetic behaviour of **1** and **2**.

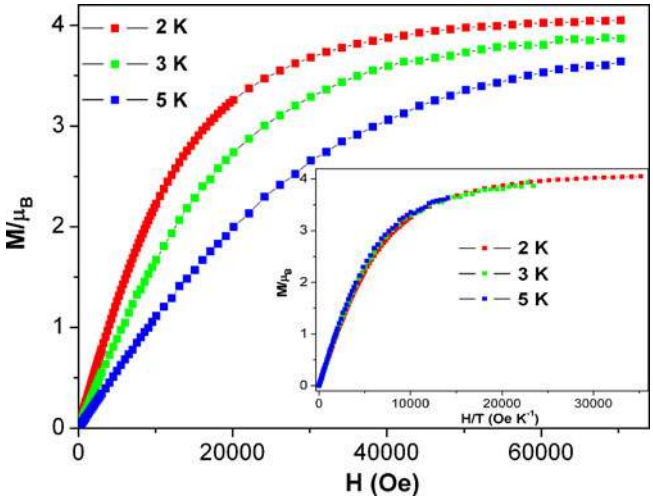

Figure 8. Plots of M *vs* H and H/T (inset) of **2** at indicated temperatures.

3.5 *EPR measurements*

The X-band EPR spectra of the complexes **1** and **2** were measured on solid powdered samples in the selected temperature range at 9.39231 GHz. The magnetic field has swept in the range of 0 to 10000 G. The nice crystals of two complexes (**1** and **2**) were grinded to make powder for EPR measurements.

The X-band EPR spectra of **1** at three different temperatures (4, 15 and 30 K) showed three major absorption peaks. The first absorption looked like a wide doublet between 0 and 3000 G followed by second broad absorption between 5000 and 6000 G and the third one was comparatively sharper at 8800 G. The number of absorptions remained same at 4 K and 30 K. The intensity of all absorption peaks gradually decreased with increasing temperature (figure 9, left). It corroborates with the zero-field-splitting as observed in the lower temperature. The X-band EPR spectra of complex **2** were completely different from that of complex **1** (figure 9). This complex (**2**) showed several major absorption peaks at 180, 1350, 3050, 4950, 9500 G due to the zero-field-splitting of the ground state. An additional absorption peak appeared at 2450 G above 25 K and became more prominent as temperature increased from 25 K to 50 K while the intensity of other absorption peaks decreased with increasing temperature. The origin of an EPR spectrum is the electronic transition between different (S, M_S) levels [(2, −2), (2, −1), (2, 0), (2, +1), (2, +2); (1, −1), (1, 0), (1, +1); (0, 0)]. S varies from $S_1 + S_2 = 2$ to $S_1 - S_2 = 0$ and for each S value M_S varies from +S to −S by an integer. Since the ZFS parameters (D) are different from each other for **1** and **2**, the splitting energy levels are not identical in **1** and **2**. Thus the positions of absorption are not same though apparently paramagnetic Ni^{II}_2 units look same in both the complexes.

Two signals between 6000 and 8800 G of **1** can be assigned to allowed transition of $\Delta M = 1$ and usually forbidden transition of $\Delta M = 2$. The related signals were also observed in **2** with a shift in the positions.[54] The complexes **1** and **2** can be put into weak exchange limit[18] as magnetic exchange parameter $J \approx 10\ cm^{-1}$ and thus the mixing between the different spin states is possible leading to the breaking of the selection rule ($\Delta S = \pm 1$). Since ZFS parameter of **2** is smaller in magnitude, the probability of mixing of spin states [such as between (2,0) and (0,0)] is more in **2**. Consequently, additional multiple signals (e.g., electronic transition) in between 2500 to 6000 G were observed for **2**.

3.6 *DFT Calculation*

To obtain a better insight on the origin and difference of the magnetic interactions in the present complexes, quantum mechanical DFT calculations were performed using *Gaussian '03* package with broken symmetry formalism. Here, our main aim was to investigate the origin and difference in magnetic behaviour of complexes **1** and **2** although both of them have almost similar dimeric magnetic core. For simplicity we reduced the structures to model complexes, as given in the figure 10. DFT calculations on both the complexes were done in two ways: (i) taking into account only two Ni(II) ions with azide bridge (figure 10, left side); and (ii) considering $Ni^{II}_2Na^{I}_2$ unit as the magnetic core (figure 10, right side). All the geometric configurations of the model complexes were taken from the experimental crystal structure data.

In both **1** and **2**, the overall multiplicity of the ground state was obtained to be 5 (quintet). The low-spin (triplet) and lowest spin (singlet) states are found to be higher

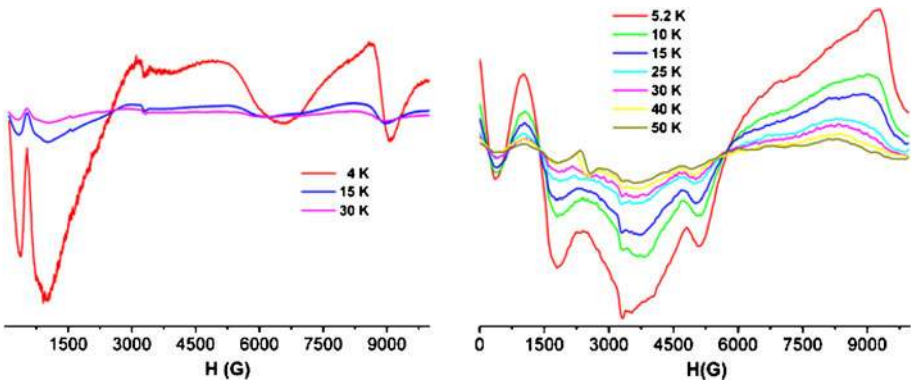

Figure 9. EPR spectra of complexes **1** (left) and **2** (right) at different temperatures.

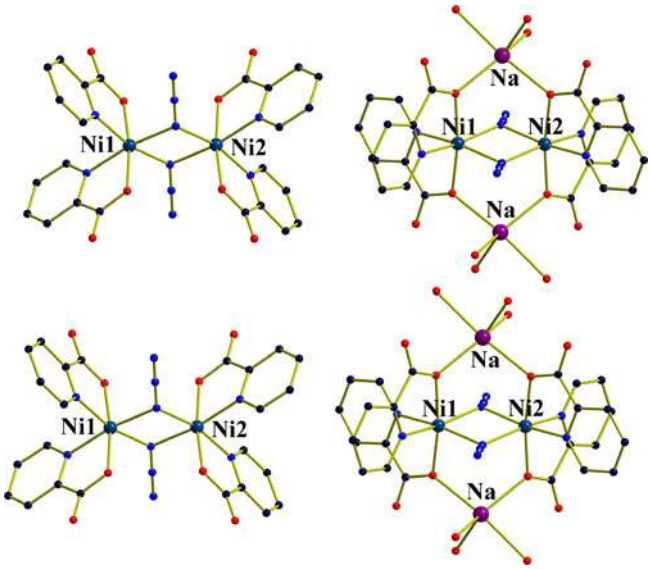

Figure 10. Model fragments of **1** (left side: considering only Ni^{II}_2 dimer; right side: considering $Ni^{II}_2Na^{I}_2$ unit) used for DFT calculation.

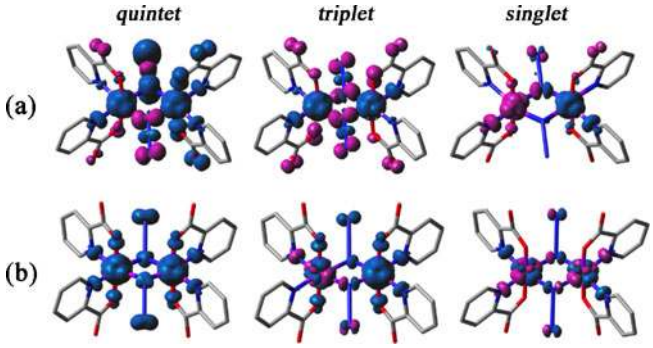

Figure 11. Spin distribution maps of **1** (**a**) and **2** (**b**) calculated in the B3LYP level for the single determinant corresponding to their each state, α and β spins are represented by blue and purple surfaces. The isodensity surfaces correspond to a value of 0.005 e/b^3.

in energy compared to the ferromagnetic high-spin state. With the Hamiltonian corresponding to Heisenberg term together with single-ion anisotropy parameter (D), energies of each spin state in terms of J and D were obtained as: E (singlet, BS; $M_s = 0$) $= +2J$; E (triplet, $M_s = 0$) $= +J + 2D/3$; and E (quintet, $M_s = 0$) $= -J - 2D$. J and D values were obtained by solving the equations of energies considering Ni^{II}_2 and $Ni^{II}_2Na^{I}_2$ cores. Results obtained considering only Ni^{II}_2 unit were $J = +20.65$ cm^{-1} and $D = -3.16$ cm^{-1} for **1**, and $J = +24.56$ cm^{-1} and $D = -4.67$ cm^{-1} for **2**. However, considering $Ni^{II}_2Na^{I}_2$ unit as magnetic core the results were $J = +16.35$ cm^{-1} (**1**), $+19.54$ cm^{-1} (**2**); $D = -3.05$ cm^{-1} (**1**), -4.25 cm^{-1} (**2**). The little difference between the experimental and theoretical results is due to fact that the experimental J and D correspond to the full three-dimensional systems, while the calculations are performed on the dimeric model structures.

The spin density distribution in magnetic systems reveals valuable information on the mechanism of magnetic interaction between the magnetic centres. The delocalization of atomic spin density of the paramagnetic centres through the bridging atom produces the magnetic coupling interactions; more delocalization gives strong interaction and less one affords weak magnetic coupling.

The Mulliken spin density analysis has been done for the complexes **1** and **2** on both Ni^{II}_2 and $Ni^{II}_2Na^{I}_2$ units (figure 11). The spin density distribution is almost similar in both the complexes in high-spin state but that is quite different in their low-spin states. The strong spin delocalization observed in complex **1** [average spin density on each Ni(II) centre is 1.48 e$^-$] in the ground quintet spin state is the indication of strong ferromagnetic interaction compared to complex **2** [average spin density on each Ni(II) centre is 1.59 e$^-$]. However, considering the $Ni^{II}_2Na^{I}_2$ unit as the magnetic core, results are close to each other. The spin density distribution was almost equal in both the complexes with average spin density value on each Ni(II) centre was 1.6 e$^-$ in both the complexes in their quintet states, which explains the reason of almost equal J values obtained experimentally for both the complexes. Very small spin density on Na(I) [average to -0.002 e$^-$ in high spin state] indicates that the effect of Na(I) in magnetic interaction is very weak. But, the negative spin density may contribute very small antiferromagnetic interaction between two Ni(II) centres through –O-Na-O-, and that was observed in the calculated J and D values. J and D become closer to the experimental results when $Ni^{II}_2Na^{I}_2$ unit was considered.

For complexes **1** and **2** the magnetic orbital analysis in their high-spin states shows that SOMOs are composed of metal d orbitals and local orbitals of the ligands. As both the complexes are isostructural, the SOMOs are almost same in both the complexes (figure S10, Supporting Information). It is evident that the $\boldsymbol{d}_{x^2-y^2}$ and $\boldsymbol{d}_{z^2}$ orbitals of Ni(II) are involved in the magnetic interactions. In both the cases the bridging ligand in the xy plane interacts with both the $\boldsymbol{d}_{x^2-y^2}$ and $\boldsymbol{d}_{z^2}$ orbitals of Ni(II) through σ fashions. The contribution of the local orbital of the bridging ligand to the magnetic orbitals is small in complex **1** compared to complex **2**. But, the strong contribution of local orbital of bridging ligand in the magnetic orbitals indicates the strong ferromagnetic interaction in both the complexes and that corroborate the experimental findings.

4. Conclusions

In conclusion, equimolar reaction of $Cu(NO_3)_2{\cdot}3H_2O$ and pyridine-2-aldehyde in methanol under refluxing condition followed by treatment with equimolar amount of 4-aminopyridine and two equivalents of NaN_3 yielded a Cu_4 cluster as $[Cu_4\{PyCH(O)(OMe)\}_4(N_3)_4]$ containing a bridging hemiacetalate ligand $[PyCH(O)(OMe)]^{-1}$.[38] Though several metal complexes of hemiacetalate of di-2-pyridyl ketone are known,[55–58] the Cu_4 cluster was the first example of a metal arrested cluster of the hemiacetalate $[PyCH(O)(OMe)]^{-1}$. Analogues attempt using Ni(II) salt was failed. However, Ni(II) salt in the presence of stronger base like NaOMe allowed the formation of 1D chains of heterometallic defect dicubane (**1** and **2**) building $Ni^{II}_2Na^{I}_2$ unit at room temperature and 100°, respectively. Similar reaction using $Cu(NO_3)_2{\cdot}3H_2O$ instead of $Ni(NO_3)_2{\cdot}6H_2O$ yielded a known heterometallic polymer $[NaCu(pic)(N_3)_2]_n$.[39] In these cases, pyridine-2-aldehyde was oxidized to corresponding pyridine-2-carboxylate in the presence of strong base. Such complexes (**1** and **2**) were not obtained when the reactions were performed directly with pyridine-2-carboxylate instead of pyridine-2-aldehyde under similar reaction condition. Hence, *in situ* oxidation has an important role in the formation of chains (**1** and **2**) with defect dicubane clusters. From magnetic point of view, complexes **1** and **2** are ferromagnetically coupled with $J \approx +10\ cm^{-1}$ and $D \approx -2$ to $-7\ cm^{-1}$ for **1** and **2**, respectively. The X-band EPR spectra of **1** and **2** are different from each other presumably due to different extent of ZFS which has been indicated from reduced magnetization *M*/*T vs H* plots of **1** and **2**. Finally DFT calculations were performed in all the cases to corroborate the experimentally obtained parameters. DFT calculations showed that in the defect cubane ($Na^{I}_2Ni^{II}_2$) core, the Ni^{II}_b-Ni^{II}_b (*body–body*) unit could be more strongly ferromagnetically coupled in the absence of diamagnetic Na^{I} ions in wing–wing positions. From magnetic point of view, the present report is important for future study of this kind of defect cubane core ($Na^{I}_2Ni^{II}_2$), because replacement of diamagnetic Na^{I} by other paramagnetic ions may lead to much interesting homo-/hetero-metallic magnetic complexes.

Supporting information

The supporting information contains X-ray crystallographic files in CIF format, fitting of magnetic (**1**) data using dimeric model. This material is available via the internet free of charge. Crystallographic data have been deposited for compounds **1–2** at the Cambridge Crystallographic Data Centre CCDC-784350 and 706448. These data can be obtained via the internet free of charge at www.ccdc.cam.ac.uk/data_request/cif, by email at data_request@ccdc.cam.ac.uk., or by contacting the Cambridge Crystallographic Data Centre, 12 Union Road, Cambridge CB2 1EZ, UK; fax: +44(0)1223–336033.

For electronic supporting information (IR spectra, χT vs T, M vs H plots and SOMOs of **1** and **2**) of figures S1–S10, see www.ias.ac.in/chemsci.

Acknowledgements

The authors acknowledge the Council of Scientific and Industrial Research (CSIR), New Delhi, and the Department of Science and Technology (DST) (SR/S1/IC-18/2008) Govt. of India for financial support to PSM. The authors acknowledge Prof. S B Bhat and his co-workers for doing X-Band EPR measurement for all three complexes.

References

1. Sessoli R, Tsai H-L, Schake A R, Wang S, Vincent J B, Folting K, Gatteschi D, Christou G and Hendrickson D N 1993 *J. Am. Chem. Soc.* **115** 1804
2. Sessoli R, Gatteschi D, Caneschi A and Novak M A 1993 *Nature* **365** 141
3. Mereacre V M, Ako A M, Clérac R, Wernsdorfer W, Filoti G, Bartolomé J, Anson C E and Powel A K 2007 *J. Am. Chem. Soc.* **129** 9248
4. Benelli C, Cano J, Journaux Y, Sessoli R, Solan G A and Winpenny R E P 2001 *Inorg. Chem.* **40** 188
5. Ako A M, Hewitt I J, Mereacre V, Clérac R, Wernsdorfer W, Anson C E and Powell A K 2006 *Angew. Chem., Int. Ed.* **45** 4926
6. Caneschi A, Gatteschi D, Sessoli R, Barra A L, Bruel L C and Guillot M 1991 *J. Am. Chem. Soc.* **113** 5873
7. Novitchi G, Wernsdorfer W, Chibotaru L F, Costes J-P, Anson C E and Powell A K 2009 *Angew. Chem., Int. Ed.* **48** 1614
8. Mishra A, Wernsdorfer W, Parson S, Christou G and Brechin E K 2005 *Chem. Commun.* 2086
9. Maspoch D, Ruiz-Molinaa D and Veciana J 2007 *Chem. Soc. Rev.* **36** 770
10. Gatteschi D and Sessoli R 2003 *Angew. Chem., Int. Ed.* **42** 268
11. Beauvais L G and Long J R 2002 *J. Am. Chem. Soc.* **124** 12096
12. Freedman D E, Harman W H, Harris T D, Long G J, Chang C J and Long J R 2010 *J. Am. Chem. Soc.* **132** 1224
13. Kahn O 1993 *Molecular magnetism* (VCH Weinheim: Germany)
14. Benelli C and Gatteschi D 2002 *Chem. Rev.* **102** 2369

15. Ginsberg A P, Brookes R W, Martin R L and Sherwood R C 1972 *Inorg. Chem.* **11** 2884
16. Journaux Y, Kahn O, Chevalier B, Etourneau J, Claude R and Dworkin A 1978 *Chem. Phys. Lett.* **55** 140
17. Joung K O, O'Connor C J, Sinn E and Carlin R L 1979 *Inorg. Chem.* **18** 804
18. Herchel R, Boča R, Krzystek J, Ozarowski A, Durán M and Slageren J V 2007 *J. Am. Chem. Soc.* **129** 10306
19. Escuer A, Vicente R, Ribas J and Solans X 1995 *Inorg. Chem.* **34** 1793
20. Mukherjee P, Drew M G B, Gómez-García J J and Ghosh A 2009 *Inorg. Chem.* **48** 5848
21. Halcrow M A, Huffman J C and Christou G 1995 *Angew. Chem., Int. Ed.* **34** 889
22. Escuer A, Front-Berdia M, Kumar S B, Solans X and Vicente R 1999 *Polyhedron* **18** 909
23. Clemente-Juan J M, Andres H, Borrás-Almenar J J, Coronado E, Gudel H U, Aebersold M, Kearly G, Buttner H and Zolliker M 1999 *J. Am. Chem. Soc.* **121** 10021
24. Yang E-C, Wernsdorfer W, Zakharov L N, Karaki Y, Yamaguchi A, Isidro R M, Lu G-D, Wilson S A, Rheingold A L, Ishimoto H and Hendrickson D N 2006 *Inorg. Chem.* **45** 529
25. Lawrence J, Yang E-C, Edwards R, Olmstead M M, Ramsey C, Dalal N S, Gantzel S, Hill P K and Hendrickson D N 2008 *Inorg. Chem.* **47** 1965
26. Venegas-Yazigi D, Canob J, Ruiz E and Alvarez S 2006 *Physica B* **384** 123
27. Habib M, Karamakar T K, Aromi G, Ribas-Arino J, Fun H-K, Chantrapromma S and Chandra S K 2008 *Inorg. Chem.* **47** 4109
28. Sarkar S, Datta A, Mondal A, Chopra D, Ribas J, Rajak J J, Sairam S M and Pati S K 2006 *J. Phys. Chem. B* **110** 12
29. Brechin E K, Clegg W, Murrie M, Parsons S, Teat S J and Winpenny R E P 1998 *J. Am. Chem. Soc.* **120** 7365
30. Mandal D, Bertolasi V, Ribas-Ariño J, Aromí G and Ray D 2008 *Inorg. Chem.* **47** 3465
31. Blake A J, Grant C M, Parsons S, Rawson J M and Winpenny R E P 1994 *J. Chem. Soc., Chem. Commun.* 2363
32. Brechin E K, Gould R O, Harris S G, Parsons S and Winpenny R E P 1996 *J. Am. Chem. Soc.* **118** 11293
33. Park I-S and Hausinger R P 1995 *Science* **267** 1156
34. Papaefstathiou G S, Perlepes S P, Escuer A, Vicente R, Font-Bardia M and Solans X 2001 *Angew. Chem., Int. Ed.* **40** 884
35. Mondal K C, Sengupta O, Nethaji M and Mukherjee P S 2008 *Dalton Trans.* 767
36. Mondal K C and Mukherjee P S 2008 *Inorg. Chem.* **47** 4215
37. Mukherjee S, Gole B, Chakrabarty R and Mukherjee P S 2009 *Inorg. Chem.* **48** 11325
38. Mondal K C, Sengupta O and Mukherjee P S 2009 *Inorg. Chem. Commun.* **12** 682
39. Goher M A S and Mautner M A 1995 *Polyhedron* **14** 1439
40. SMART/SAINT, Bruker AXS 2004 Inc.: Madison WI
41. Sheldrick G M, SHELX-97 1998 *Program for the Solution and Refinement of Crystal Structures* (University of Göttingen, Göttingen, Germany)
42. Barbour L J 2001 *J. Supramol. Chem.* **1** 189
43. Farrugia L J 2003 WinGX: An Integrated System of Windows Programs for the Solution, Refinement and Analysis for Single Crystal X-ray Diffraction Data, version 1.65.04; Department of Chemistry: University of Glasgow (Farrugia L J 1999 *J. Appl. Crystallogr.* **32** 837)
44. Sheldrick G M 1999 SADABS Bruker Nonius Area Detector Scaling and Absorption Correction, version 2.05; University of Göttingen, Göttingen, Germany
45. Ruiz E, Alemany P, Alvarez S and Cano J 1997 *J. Am. Chem. Soc.* **119** 1297
46. Ruiz E, Rodríguez-Fortea A, Cano J, Alvarez S and Alemany P 2003 *J. Comput. Chem.* **24** 982
47. Ruiz E, Cano J, Alvarez S and Alemany P 1998 *J. Am. Chem. Soc.* **120** 11122
48. Becke A D 1993 *J. Chem. Phys.* **98** 5648
49. Frisch M J, Trucks G W, Schlegel H B, Scuseria G E, Robb M A, Cheeseman J R, Montgomery J A, Vreven T, Kudin K N, Burant J C, Millam J M, Iyengar S S, Tomasi J, Barone V, Mennucci B, Cossi M, Scalmani G, Rega N, Petersson G A, Nakatsuji H, Hada M, Ehara M, Toyota K, Fukuda R, Hasegawa J, Ishida H, Nakajima T, Honda Y, Kitao O, Nakai H, Klene M, Li X, Knox J E, Hratchian H P, Cross J B, Adamo C, Jaramillo J, Gomperts R, Stratmann R E, Yazyev O, Austin A J, Cammi R, Pomelli C, Ochterski J, Ayala P Y, Morokuma K, Voth G A, Salvador P, Dannenberg J J, Zakrzewski V G, Dapprich S, Daniels A D, Strain M C, Farkas O, Malick D K, Rabuck A D, Raghavachari K, Foresman J B, Ortiz J V, Cui Q, Baboul A G, Clifford S, Cioslowski J, Stefanov B B, Liu G, Liashenko A, Piskorz P, Komaromi I, Martin R L, Fox D J, Keith T, Al-Laham M A, Peng C Y, Nanayakkara A, Challacombe M, Gill P M W, Johnson B, Chen W, Wong M W, Gonzalez C and Pople J A 2003 Gaussian 03, revision B.4; Gaussian Inc.: Pittsburgh, PA
50. Becke A D 1988 *Phys. Rev. A* **38** 3098
51. Lee C, Yang W and Parr R G 1988 *Phys. Rev. B* **37** 785
52. Ruiz E, Alvarez S, Cano J and Polo V 2005 *J. Chem. Phys.* **123** 164110
53. Ribas J, Escuer A, Monfort M, Vicente R, Cortes R, Lezama L and Roji T 1999 *Coord. Chem. Rev.* **193–195** 1027
54. Cortés R, Lezama L and Rojo T 1994 *IEEE Trans. Magn.* **30** 4728
55. Deveson A C, Heath S L, Harding C J and Powell A K 1996 *J. Chem. Soc., Dalton Trans.* 3173
56. Papadopoulos A, Tangoulis V, Raptopoulou C P, Terzis A, Kessissoglou D P 1996 *Inorg. Chem.* **35** 559
57. Bradford P, Hynes R C, Payne N C and Willis C J 1990 *J. Am. Chem. Soc.* **112** 2647
58. Tangoulis V, Paschalidou S, Bakalbassis E G, Perlepes S P, Raptopoulou C P and Terzis A T A 1997 *Angew. Chem., Int. Ed.* **36** 1083